Available online at www.sciencedirect.com
SCIENCE DIRECT®
Journal of volcanology and geothermal research
ELSEVIER
Journal of Volcanology and Geothermal Research 152 (2006) 109–120
www.elsevier.com/locate/jvolgeores

Electrical properties of hydrothermally altered dacite from the PACMANUS hydrothermal field (ODP Leg 193)

Anne Bartetzko [a,b,*], Norbert Klitzsch [a], Gerardo Iturrino [c], Stephan Kaufhold [d], Juliane Arnold [a]

[a] *Applied Geophysics, RWTH Aachen, Lochnerstr. 4-20, 52066 Aachen, Germany*
[b] *Research Center Ocean Margins, Department of Geosciences, University of Bremen, P.O. Box 330440, 28334 Bremen, Germany*
[c] *Borehole Research Group, Lamont–Doherty Earth Observatory, 61 Route 9W, Palisades, NY 10964-1000 USA*
[d] *Bundesanstalt für Geowissenschaften und Rohstoffe, Stilleweg 2, 30655 Hannover, Germany*

Received 1 February 2005; received in revised form 16 August 2005; accepted 13 October 2005
Available online 23 November 2005

Abstract

Ocean Drilling Program Leg 193 drilled two sites at the PACMANUS hydrothermal field, Snowcap and Roman Ruins. We investigated electrical properties of core samples recovered from these sites to study the effect of hydrothermal alteration on the electrical properties of dacite. Most of the samples are completely altered and have a high porosity (0.16–0.43). When saturated with seawater, they have a high electrical conductivity (0.05–0.3 S/m) and low formation factor (12–103). The only fresh sample has a low porosity (0.01), low electrical conductivity (0.002 S/m), and high formation factor (1920). The samples show a wide range in tortuosity, which can be explained by the large variety of volcanic textures and changes in pore space structure due to hydrothermal alteration. Samples from the Roman Ruins field that exhibit siliceous and sulfate–silica–clay alteration styles have a high surface conductivity, which is related to high clay contents and the presence of clay minerals with high cation exchange capacity such as vermiculite and surface conductivity has a significant effect on formation factor values. In contrast, siliceous samples from the Snowcap field have lower surface conductivity, clay content, and cation exchange capacities. Borehole conductivity measurements (induction log) indicate a non-negligible influence of electronic conduction due to the presence of sulfide minerals. This indication is confirmed by laboratory measurements: several samples show a high frequency dependence in their electrical properties which is probably related to the presence of disseminated pyrite. Intense fracturing, brecciation, high porosity, hydrothermal alteration and the presence of pyrite mineralization are the main factors controlling electrical conductivity of the hydrothermally altered formation.
© 2005 Elsevier B.V. All rights reserved.

Keywords: Ocean Drilling Program; Leg 193; electrical properties; formation factor; dacite; hydrothermal alteration

1. Introduction

Leg 193 was the Ocean Drilling Program's (ODP) first endeavor drilling into an active hydrothermal vent field associated with felsic magmatism at a convergent plate margin. Leg 193 drilled the PACMANUS hydrothermal field (**P**apua New Guinea–**A**ustralia–**C**anada–**Manus**), situated in the eastern Manus basin, Papua

* Corresponding author. Present address: Research Center Ocean Margins, Department of Geosciences, University of Bremen, P.O. Box 330440, 28334 Bremen, Germany. Tel.: +49 421 218 65809; fax: +49 421 218 65810.
E-mail address: bartetzko@uni-bremen.de (A. Bartetzko).

0377-0273/$ - see front matter © 2005 Elsevier B.V. All rights reserved.
doi:10.1016/j.jvolgeores.2005.10.002

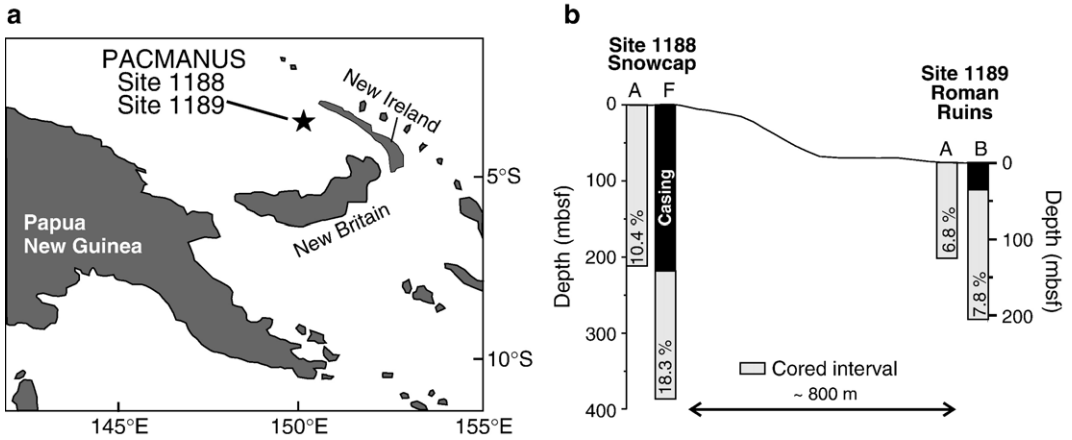

Fig. 1. (a) Location of ODP Leg 193 drill sites in the PACMANUS hydrothermal field, eastern Manus basin, Papua New Guinea (modified after Binns et al., 2002). (b) Overview of the boreholes sampled for this study at Site 1188 (Snowcap) and Site 1189 (Roman Ruins). Letters above the seafloor represent the ODP name classification for boreholes drilled at each site. The numbers at the bottom of the holes give the average core recovery and mbsf is defined as meters below sea floor.

New Guinea (Fig. 1a). It was discovered in 1991 (Binns and Scott, 1993), and consists of several isolated hydrothermal deposits lined along the crest of a felsic neovolcanic ridge, Pual Ridge. Two of these deposits were drilled during Leg 193 (Fig. 1b). One site, Snowcap (Site 1188), is characterized by diffuse low-temperature venting (~6 °C) at the surface, while the other site, Roman Ruins (Site 1189), consists of numerous black smoker chimney structures discharging hot hydrothermal fluids (220–276 °C). The rocks drilled at both sites are of dacitic to rhyodacitic composition (Binns et al., 2002).

With the exception of some unaltered lava flows at the top of the Snowcap hydrothermal field, these rocks are highly to completely altered, i.e. more than 80% of the original material is replaced by secondary minerals. Hydrothermal alteration at PACMANUS is complex and multi-stage, where several episodes of fracturing and fluid flow result in multiple veining and alteration events. Pervasive alteration of the groundmass or localized altered patches along halos and veins have been observed along with massive to semi-massive sulfides and stockwork sulfide mineralization, particularly in the cores from Hole 1189B (Binns et al., 2002).

ODP Leg 193 offers a unique opportunity to study the effect of high-temperature hydrothermal activity on the physical properties of dacitic rocks, especially since these environments have not been particularly well characterized. In this manuscript, we present a compilation of electrical conductivity measurements carried

Table 1
List of samples analyzed in this study and the samples analyzed at NER (Iturrino et al., 2004). GSC = green silica clay alteration, SSC = silica sulfate clay alteration. Information on alteration is compiled from Binns et al. (2002)

Hole	Sample (core-section, cm)	Depth (mbsf)	Vesicularity	Alteration intensity	Alteration style	Laboratory
1188A	3R-1, 13–15	19.33	Moderately	Fresh	Film	NER
1188A	7R-2, 76–79	50.46		Completely	Siliceous/GSC	NER
1188A	9R-1, 118–120	68.78		Completely	Bleaching	NER
1188A	14R-1, 102–104	117.02		Completely	Bleaching/siliceous	NER
1188A	16R-2, 46–48	137.31	Sparsely	Completely	GSC	NER
1188A	17R-2, 29–31	146.89	Sparsely	Completely	GSC	NER
1188F	25Z-1, 12–14	295.72		Completely	Siliceous	Aachen
1188F	26Z-1, 8–10	300.18		Completely	Siliceous	Aachen
1189A	8R-1, 87–90	68.87		Completely	Siliceous	NER
1189B	11R-2, 20–22	128.45	Slightly	Completely	SSC/siliceous	Aachen
1189B	11R-2, 117–119	129.42	Slightly	Completely	SSC/siliceous	Aachen
1189B	11R-3, 12–14	130.72	Moderately	Completely	SSC/siliceous	NER
1189B	12R-1, 11–13	137.41	Slightly	Completely	SSC/siliceous	Aachen
1189B	12R-2, 65–67	139.36	Slightly	Completely	SSC/siliceous	Aachen
1189B	15R-1, 63–65	166.73		Completely	Siliceous/SSC	NER

out in two different laboratories on variably altered core samples from the Snowcap (Holes 1188A and 1188F) and the Roman Ruins (Holes 1189A and 1189B) fields. Samples selected for this study represent most of the observed alteration styles (Table 1); however, no samples with pronounced sulfide mineralization were available due to low core recovery (<1–2%) in the mineralized intervals.

Measurements on six samples were performed with saturating fluids of varying salinity and thus conductivity. These measurements were undertaken to investigate the influence of surface conductivity on rock conductivity and to determine formation factors. Surface conductivity is related to inner surface area and hence to clay content. Because of the high amount of clay in these hydrothermally altered rocks, surface conductivity was expected to play an important role. These experiments also measured cation exchange capacity, which provides complementary information about the rock's inner surface. In order to gather more information, this data set was complemented by measurements on nine samples carried out at the New England Research Laboratory (NER) in Vermont. Those measurements focused on electrical resistivity as a function of frequency using a constant fluid salinity.

2. Electrical conductivity of rocks

In a porous rock consisting of a non-conducting matrix, the electrical conductivity is controlled by both the electrolytic conduction of the fluid in the connected pore space and by surface conduction at the interface between fluid and mineral grains. In the case of negligible surface conduction, the electrical conductivity of the rock σ_{rock} depends on the conductivity of the fluid σ_{fluid} and on the inner rock structure, represented by the formation factor F:

$$F = \frac{\sigma_{\text{fluid}}}{\sigma_{\text{rock}}} \tag{1}$$

For sedimentary rocks, an empirical relationship was described by Archie (1942) to relate formation factor and porosity ϕ:

$$F = a\phi^{-m} \tag{2a}$$

The parameters a and m are theoretically constant for an individual rock type. Originally it was assumed $a=1$, but it was later found that a required modification in order to fit experimental data. The exponent m is often called the "cementation exponent," but several studies have shown that it is frequently not related to the cementation of a sediment. Instead, a number of structural parameters influence the parameter m, such as the shape of the grains (e.g. Jackson et al., 1978; Mendelson and Cohen, 1982), the shape of the pores (e.g. Ransom, 1984), and the degree of network connectivity (e.g. Purvance and Andricevic, 2000). In this study, we consider a model-based approach for the formation factor. The pores are assumed to be cylindrical pores situated in periodic arrays (Kan and Sen, 1987). In this case, the formation factor can be described as the ratio of tortuosity a to porosity ϕ:

$$F = a/\phi \tag{2b}$$

This corresponds to the Archie equation with the cementation exponent m equal to 1, i.e. the entire pore space is considered to contribute equally to the transport of the electrical current. The tortuosity is a geometric description of the rock and takes into account the tortuous paths around the mineral grains. The simplest model considers the tortuosity as the square of the ratio of pore path length to sample thickness. In more sophisticated approaches, the tortuosity also accounts for the constrictivity of the pores (variations in pore cross sectional area) and the connectivity of the pore space (e.g. Van Brakel and Heertjes, 1974; Guégen and Palciauskas, 1994).

Although originally developed for sediments, Archie's law has also been used in igneous environments (e.g. Pezard, 1990; Jarrard and Schaar, 1991; Ildefonse and Pezard, 2001). Results of these studies show that the electrical conductivity of igneous rocks is primarily controlled by the void space, i.e. by the fracture network. However, these studies also indicate that clay minerals, the alteration products of igneous rocks, increase electrical conductivity via surface conduction.

Revil et al. (1998, 2002) developed a model to explain conduction mechanisms in shaly sands and zeolitized volcaniclastic rocks. This model considers two electrical conduction mechanisms: (a) electrical conductivity through electromigration of cations and anions through the connected pore space, and (b) migration of weakly adsorbed counterions (primarily cations) at the pore water–mineral interface. At high pore fluid salinity, electromigration through the pore space is the principal mechanism of conduction, while surface migration dominates at low pore fluid salinity. Based on this microscopic model, Revil et al. (1998) proposed an expression (Eq. 11 in Revil et al., 1998) for the macroscopic conductivity using the Hanai–Bruggemann equation. Assuming $m=1$, according to our model-based approach for the formation factor (Eq.

(2b)), the equation can be solved for the macroscopic conductivity:

$$\sigma = \frac{\sigma_{\text{fluid}}}{F}\left[1 + (F-1)\frac{\sigma_{\text{surface}}}{\sigma_{\text{fluid}}}\right] \quad (3)$$

The surface conductivity σ_{surface} is mainly determined by the cation exchange capacity (CEC) of the clay minerals in the rock. The CEC gives the maximum number of surface exchangeable cations per unit mass and is an important parameter for clay minerals. It strongly depends on the content of swelling clay minerals, as they have a much larger specific inner surface than other clay minerals (e.g. Patchett, 1975). In clay-rich rocks with relatively small amounts of swelling clay minerals (5–15 wt.%; e.g. smectite, CEC ~80–150 meq/100 g) in comparison with other clay minerals such as illite (CEC ~10–40 meq/100 g) or kaolinite (40–80 wt.%; CEC 3–15 meq/100 g), the electrical conductivity is still highly dependent on the amount of swelling clay minerals present, rather than on the presence of illite and/or kaolinite, which may have a contribution of only 10% to the CEC (Grim, 1968; Kaufhold and Penner, 2004).

Frequency influences electrical conductivity as a result of electrical polarization processes inside the rock (e.g. Pelton, 1977; Titov et al., 2002). This polarization is due to the time-limited charge transfer (electrode polarization) at the interface between a metal and a fluid, and due to ion transport differences in wide and narrow pores (membrane polarization) between a non-metal (e.g. clay mineral) and a fluid. The conduction of weakly adsorbed cations at the mineral surface is responsible for the ion transport difference because the majority of cations contribute to the overall electrical conduction in narrow pores. Electrode polarization generally produces a larger effect than membrane polarization. The relaxation frequency (or relaxation time) is determined by structural parameters (grain or pore size distribution).

3. Methodology

Electrical conductivity was measured at RWTH Aachen on saturated cylindrical minicore samples 2.54 cm in diameter and 2–3 cm in length. Two current electrodes were placed on the faces of the minicore. Each current electrode consisted of a stainless steel plate of 3 cm in diameter. To ensure a good contact between the rock sample and each electrode, a thin sponge saturated with fluid of matching salinity as used for the specimen was placed between the two. Two thin copper wires were wrapped around the sample (distance between the wires 1 cm) to measure electrical potential. Using the '4-point light' measuring device by Lippmann–Geophysikalische Meßgeräte, a constant current I of 100 nA for low fluid salinity and of 1 μA at high salinity, with a frequency of 8.3 Hz, was introduced through the samples. The potential difference U between the copper wires was measured. The conductivity σ_{sample} is determined by:

$$\sigma_{\text{sample}} = L/A \cdot I/U \quad (4)$$

A is the cross-section of the sample and L is the distance between the copper wires.

Electrical conductivity measurements were carried out on samples saturated with NaCl solution of varying salinities: demineralized water (~0.0003 M), 0.01 M, 0.1 M, seawater (~0.6 M), 1 M, and saturated (~2.9 M). The core samples were first cleaned in demineralized water to dissolve salts in the pore space that had crystallized as the samples were shipped dry from the core repository. Between the different saturation steps, the samples were cleaned as before, again dried at 40–50 °C for at least 72 h, saturated under vacuum and let equilibrate for several days. Fluid conductivity was controlled after saturation and during equilibration. Five measurements of electrical conductivity were performed at each salinity and averaged. All measurements were carried out under laboratory conditions (i.e. room temperature and atmospheric pressure).

Porosity was measured by determining the volume of the samples and the volume of the solid rock (i.e. matrix) using two pycnometers. The volume of the dry solid material was measured with a helium pycnometer (Accupyc™; Micromeritics, 2001a). The use of helium as displacing fluid assures penetration into very small pores. After determining the weight of the samples, the density of the solid material was calculated (d_{matrix}). The total dry sample volume was measured with a pycnometer that uses a synthetic material called *DryFlo*™ (Geopyc™, Micromeritics, 2001b). The measurements were carried out once without the sample and once with the dry sample. The difference between the two measurements gives the sample volume, and as the weight of the sample is known, the dry bulk density (d_{bulk}) can be calculated. Porosity (ϕ) is then calculated by

$$\phi = \frac{d_{\text{matrix}} - d_{\text{bulk}}}{d_{\text{matrix}}} \quad (5)$$

The error of the porosity determined in the described way is less than 3%.

Measurements of the CEC were carried out at Bundesanstalt für Geowissenschaften und Rohstoffe (BGR), Hannover, Germany. To determine the CEC, the naturally occurring cations are completely exchanged by specific ions or complexes. The Cu_{triene} method (Meier and Kahr, 1999) was applied in this study and uses a stable complex of copper (II) ions with triethylentetramine (triene). The CEC is obtained in units of meq/100 g (milliequivalents/100 g).

At NER, electrical conductivity measurements on a total of 9 samples were made as a function of frequency. All the samples were saturated with a 31 g/l sea salt solution under vacuum and equilibrated individually. Measurements were carried out at room temperature. The samples were first pressurized to approximately 5 MPa effective confining pressure (confining pressure of 10 MPa, pore pressure of 5 MPa) and allowed to equilibrate to that stress. Electrical properties were then measured using an NER ZMeter impedance analysis system using a four-electrode configuration (Lockner and Byerlee, 1985). Data was collected at frequencies ranging from 0.1 to 100,000 Hz. The formation factor was determined at a frequency of 8 Hz for one sample (sample 1188A-3R-1, 13–15) and at 10 Hz for all other samples. A detailed description of the methodology is available from Iturrino et al. (2000, 2004).

4. Results

The results of electrical conductivity measurements with varying fluid salinities are pointed out in Table 2 and shown in Fig. 2. All samples show the typical increase in rock conductivity with increasing fluid conductivity at fluid conductivities greater than 0.2 S/m, and all samples show similar electrical conductivity values. At low fluid conductivities (<0.2 S/m), the surface conduction dominates, and differences between the samples are larger. The two samples from the Snowcap area have lower conductivities than the ones from Roman Ruins field. Porosity values (Eq. (5)) range from 0.16 to 0.22 (Table 3). This narrow range in porosity is consistent with the narrow range in sample electrical conductivity at high fluid conductivity. This suggests that at high fluid conductivity, sample conductivity is mainly controlled by the conductivity of the saturating fluid and thus porosity of the rock. The formation factor was computed using the values measured at the given seawater concentrations (Table 3). Formation factor values derived using Eq. (3), which considers surface conduction, are higher than values calculated using Eq. (1) (Table 3). However, values based on Eq. (1) are used to enable comparison with samples measured at NER.

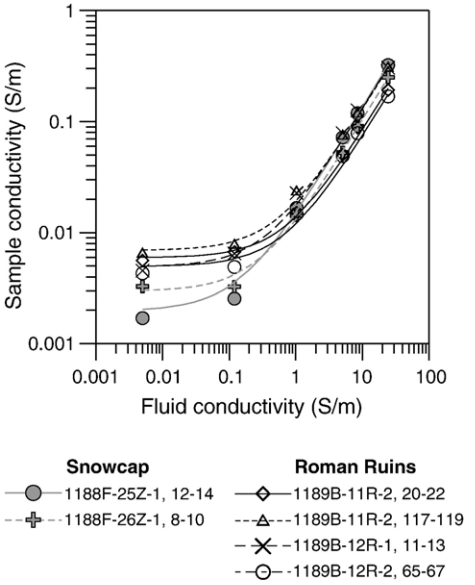

Fig. 2. Sample electrical conductivity plotted versus electrical fluid conductivity. Measured data are plotted as marks. Lines represent fits using Eq. (3) for the individual samples.

The CEC varies between 0.5 and 8.9 meq/100 g (Table 3), and the values from the Snowcap field are

Table 2
Mean value and standard deviation (Std.d) of electrical conductivity (in millisiemens per meter) of 5 repeated measurements on core samples saturated with fluids of different salinity

Sample (core-section, cm)	Demineralized water (0.005 S/m)		0.01 M (0.12 S/m)		0.1 M (1.03 S/m)		Seawater (5.08 S/m)		1 M (8.49 S/m)		Saturated (24.4 S/m)	
	Mean	Std.d	Mean	Std.d	Mean	Std.d	Mean	Std.d	Mean	Std.d	Mean	Std.d
1188F-25Z-1, 12–14	1.70	0.10	2.57	0.30	16.74	0.57	72.87	8.83	119.8	12.28	322.9	17.38
1188F-26Z-1, 8–10	3.31	0.35	3.28	0.22	14.40	1.16	53.00	5.32	92.17	10.63	251.5	11.56
1189B-11R-2, 20–22	5.64	0.52	6.85	1.13	15.30	1.69	50.75	4.98	89.29	8.85	196.7	29.48
1189B-11R-2, 117–119	6.43	0.30	7.74	0.75	23.46	1.61	74.62	5.88	117.8	6.50	301.8	23.08
1189B-12R-1, 11–13	4.55	0.21	6.54	0.54	22.76	1.23	78.76	4.35	127.7	11.26	309.9	40.00
1189B-12R-2, 65–67	4.33	0.36	4.92	0.30	14.67	0.91	49.41	5.71	78.76	4.33	169.5	14.11

Table 3
Results for electrical conductivity, porosity, formation factor, and CEC for samples analyzed in this study and analyzed at NER (Iturrino et al., 2004)

Hole	Sample (core-section, cm)	Electrical conductivity (S/m)[1]	Porosity	Formation factor, Eq. (1)[2]	Formation factor, Eq. (3)	CEC (meq/100 g)	Permeability (m^2, at 10 MPa, Iturrino et al., 2004)
1188A	3R-1, 13–15	0.002	0.01	1920			1.17 E-14
1188A	7R-2, 76–79	0.185	0.32	19			2.23 E-17
1188A	9R-1, 118–120	0.167	0.30	23			1.04 E-16
1188A	14R-1, 102–104	0.303	0.43	12			2.00 E-15
1188A	16R-2, 46–48	0.094	0.21	39			1.50 E-15
1188A	17R-2, 29–31	0.123	0.24	29			4.46 E-16
1188F	25Z-1, 12–14	0.072	0.16	70 ± 8	76	0.5	
1188F	26Z-1, 8–10	0.053	0.17	96 ± 10	99	1.0	
1189A	8R-1, 87–90	0.313	0.38	12			7.59 E-16
1189B	11R-2, 20–22	0.050	0.17	100 ± 10	126	6.5	
1189B	11R-2, 117–119	0.074	0.22	68 ± 5	82	7.1	
1189B	11R-3, 12–14	0.056	0.22	56			1.25 E-17
1189B	12R-1, 11–13	0.079	0.20	65 ± 4	79	6.7	
1189B	12R-2, 65–67	0.049	0.21	103 ± 12	143	8.9	
1189B	15R-1, 63–65	0.130	0.24	29			4.48 E-17

[1] Seawater as saturating fluid.
[2] Error for formation factors were calculated by error propagation using the standard deviation of the electrical conductivity measurements (Table 2).

significantly lower (0.5 and 1 meq/100 g) than those from the Roman Ruins field (6.5–8.9 meq/100 g). This result is consistent with the lower surface conductivity of the samples from the Snowcap field.

Results of the frequency-dependent measurements are shown in Fig. 3. Electrical conductivity, formation factor and porosity values are given in Table 3. Five of the nine samples show only a slight decrease in forma-

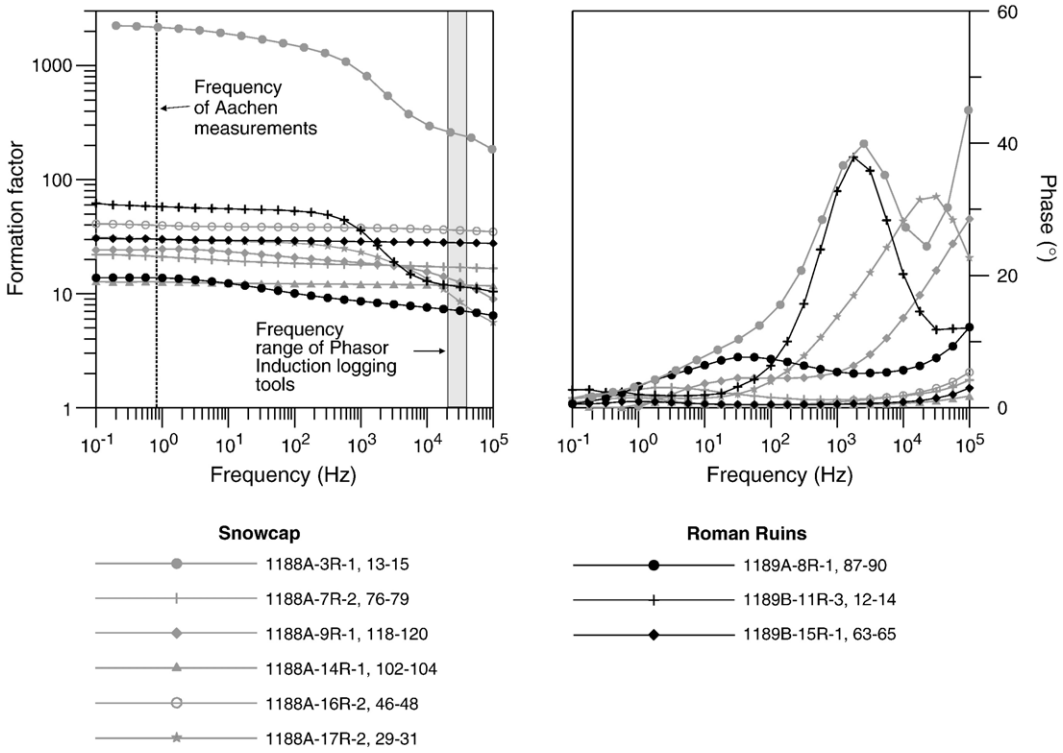

Fig. 3. Formation factor and phase versus frequency for the measurements carried out at NER. Four of the nine samples show a considerable frequency dependency of electrical conductivity.

tion factor with frequency. The other four samples (1188A-3R-1, 13–15; 1188A-9R-1, 118–120; 1188A-17R-2, 29–31; and 1189B-11R-3, 12–14) show strong decreases in formation factor with frequency and considerable phase shifts.

5. Interpretation and discussion

5.1. Porosity and formation factor

Most of the samples analyzed at RWTH Aachen and NER have electrical conductivity values between 0.05 and 0.3 S/m, porosities between 0.16 and 0.43, and formation factor values between 12 and 103 (for seawater as the saturating fluid). The only fresh sample (sample 1188A-3R-1, 13–15) has a very low electrical conductivity value (0.002 S/m), a very low porosity value (0.01), and a high formation factor (1920). The samples measured at RWTH Aachen tend to have slightly higher formation factor values within the same porosity range than the ones measured at NER. However, this may be explained by sampling a relatively small interval, as four of the six samples analyzed in Aachen are from a short, 12 m long interval in Hole 1189B. Despite the differences in methodology and pressure conditions, there is a high conformity between the results obtained at both laboratories. However, Iturrino et al. (2004) demonstrated that, within the applied pressure range, confining pressure does not have a significant influence on the electrical conductivity of the samples.

Fig. 4 shows plots of formation factor versus porosity for the dacite samples analyzed in this study (Fig. 4a) and in comparison to values for volcanic rocks obtained from other studies (Fig. 4b). The data show the typical decrease in formation factor with increasing porosity, values from the several sources depicted agree remarkably well.

In Fig. 4a we plotted an upper and lower boundary for the tortuosity (Eq. (2b)) of the Leg 193 samples. These samples cover a broad range in tortuosity from 4.4 to 27.5. The high tortuosity values can be related to the fact that the measured porosity used in this study does not correspond to the effective porosity as required by Eq. (2b). Almost the entire volcanic data set falls within the range of tortuosity values observed in the samples analyzed in this study. This indicates that the samples from the PACMANUS field exhibit a wide range in tortuosity representative for a variety of volcanic textures. They overlap particularly well with values for basalts from ODP Leg 124 investigated by Jarrard and Schaar (1991) and with zeolitized volcani-

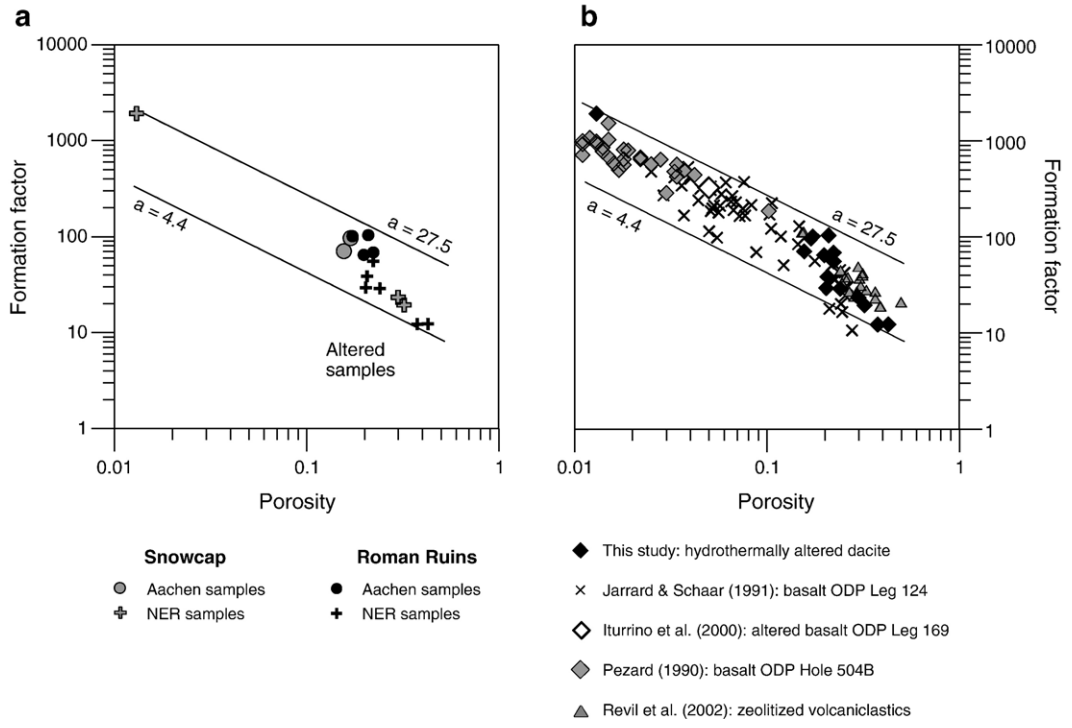

Fig. 4. Plots of formation factor versus porosity for (a) the samples from this study and (b) in comparison to results from similar measurements made on volcanic rocks from different studies. Functions were calculated according to Eq. (2b).

clastics analyzed by Revil et al. (2002). Basalts cored during ODP Leg 124 are also from a back-arc environment and those from Hole 768C are characterized by high amounts of vesicles (30–50%) that are partly filled with secondary minerals (Rangin et al., 1990). The volcaniclastic rocks analyzed by Revil et al. (2002) are diagenetic and hydrothermally altered tuff samples where secondary mineral phases such as zeolites and clays replaced the primary phases of rhyodacitic to rhyolithic composition. In the Leg 193 samples, the original volcanic texture is preserved in many samples despite the strong hydrothermal alteration, (Binns et al., 2002; Paulick et al., 2004). The samples represent massive coherent vesicular dacite (e.g. samples from cores 1189B-11R and 1189B-12R), flow banding textures (samples 1188A-7R-2, 76–79; 1188A-16R-2, 46–48; and 1189B-15R-1, 63–65), or brecciation (sample 1189B-15R-1, 63–65). This variety in volcanic texture is related to the complex volcanic architecture that is characterized by small-scale facies changes and emplacement of small-volume individual lava flows (Bartetzko et al., 2003; Paulick et al., 2004). These different textures are related to different eruption and emplacement conditions which can result in different pore space morphologies, e.g. frequency, shape, and size of vesicles and other void spaces (e.g. Saar and Manga, 1999; Smith et al., 2001; Sruoga et al., 2004). Moreover, multiple alteration stages, with extensive replacement of the original igneous mineral phases by secondary alteration products and recrystallization processes, modified the pore space structure of the rocks. Christiansen and Iturrino (2004) observed a decrease in porosity with depth at the Snowcap site and attributed it to the increasing amount of quartz with depth that fills void spaces due to hydrothermal alteration. Ketcham and Iturrino (2005) concluded from high-resolution X-ray computed tomography (CT) scans and permeability measurements on Leg 193 samples (the same sample set as analyzed at NER) that permeability is a result of pervasive replacement processes with subsequent stages of fracturing and mineral precipitation. For example, CT scans show a uniform effective microporosity in sample 1189B-11R-3, 12–14, which is interpreted as a result of chlorite and other alteration products replacing the original mineralogy. Two samples (1188A-9R-1, 118–120 and 1189A-8R-1, 87–90) show quartz–pyrite veins that built low-porosity barriers but may have precipitated along former fluid conduits.

Fig. 4 shows that tortuosity is a decreasing function of porosity for porosities higher than 0.2. This trend is expected because for a porosity of one (only fluid is present), the formation factor should also be equal to one, which implies a tortuosity of one (Eq. (2b)). The observed decrease of tortuosity with increasing porosity in the high porosity range suggests significant changes in pore space structure. A possible explanation is that the likelihood of connections between pores rises at higher porosity. At the low end of the porosity spectrum, data plotted in Fig. 4 tend towards higher tortuosity values. Sample 1188A-3R-1, 13–15 is the only sample analyzed in this study that falls into the low porosity field and is also one of the samples with the highest tortuosity. Macroscopically, this sample is moderately vesicular, but measured porosity is low (0.01; Iturrino et al., 2004) while CT scans indicate a higher porosity (~0.05; Ketcham and Iturrino, 2005). Permeability of this sample is high compared to the other samples (1.7E-14; Table 3), which is in contrast to its low porosity and low electrical conductivity. Nevertheless, the difference in measured porosity and porosity derived from CT scans indicates a low connectivity in this sample, which accounts for its high tortuosity. An isolated porosity does not account for tortuosity and is not considered in Eq. (2b).

5.2. Effect of hydrothermal alteration on electrical conductivity

The sample with the lowest electrical conductivity (0.002 S/m; sample 1188A-3R-1, 13–15) is the only fresh one included in this study. It has only minor alteration patches (Table 1; Binns et al., 2002). The low connected porosity and slight degree of alteration explain the low electrical conductivity. This sample belongs to a unit of fresh lava flows at the Snowcap site that cover the underlying, strongly hydrothermally altered rocks (Binns et al., 2002).

All other samples are completely altered and 95% to 100% of the primary igneous mineral phases have been replaced by secondary alteration mineral phases (Table 1; Binns et al., 2002). Samples are from depth intervals that show beaching, green silica clay (GSC) alteration, silica sulfate clay (SSC) alteration and/or siliceous alteration. Dominant alteration minerals are silica (25–85%), clay (8–55%), and sulfate (14–30%). Clay minerals commonly found at these depth intervals are chlorite, illite, chlorite–vermiculite, chlorite–smectite, illite–smectite, illite–vermiculite mixed layer clays and also monomineralic pyrophyllite within the bleached intervals (Lackschewitz et al., 2004).

Fig. 5 shows a plot of surface electrical conductivity versus clay content and CEC for the samples measured

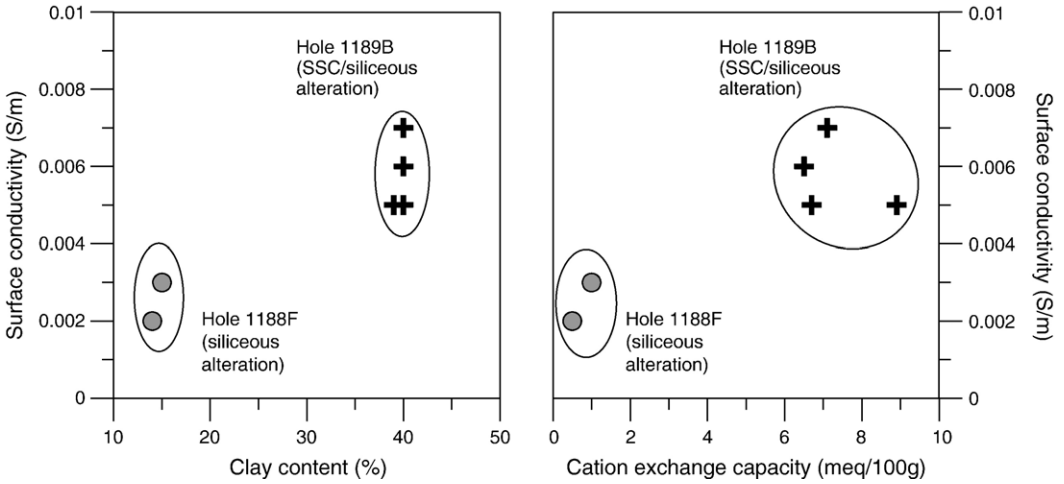

Fig. 5. Relationship between surface electrical conductivity, clay content and cation exchange capacity. Surface conductivity values are derived by fitting Eq. (3) to the data shown in Fig. 2. Clay content values were obtained from Binns et al., 2002.

at RWTH Aachen. The two samples from the Snowcap Site are similar in surface electrical conductivity (0.002 and 0.003 S/m), clay content (~15%), and CEC (0.5 and 1 meq/100 g). Also, the four samples from the Roman Ruins Site have similar surface electrical conductivity (0.005 to 0.007 S/m), clay content (~40%) and CEC values (6.5–8.9 meq/100 g). Surface electrical conductivity, clay content, and CEC are significantly higher in the Roman Ruins samples than in the Snowcap samples. The two samples from the Snowcap Site are from a narrow (~5 m) interval with siliceous alteration, characterized by high contents of silica (85%) and clays (14–15%) including chlorite, illite, and illite–chlorite mixed-layers (Binns et al., 2002; Lackschewitz et al., 2004). The samples from the Roman Ruins site are from a depth interval with silica–sulfate–clay (SSC) and siliceous types of alteration. Typical secondary alteration mineral phases of this interval are quartz (58–70%) and clay minerals (30–40%). The clay mineral phase of this depth interval does not contain chlorite and illite, but instead chlorite–vermiculite and illite–vermiculite mixed layer clay minerals (Binns et al., 2002; Lackschewitz et al., 2004). Differences in surface electrical conductivity and CEC between the two sites can to some degree be explained by the higher clay content in the samples from the Roman Ruins site. However, clay mineral content is 2–3 times higher while CEC is 6–9 times higher in the samples from the Roman Ruins site than in the samples from the Snowcap. The most likely explanation for the significantly higher CEC in the samples from the Roman Ruins site is the different composition of the clay mineral phase, e.g. the presence of vermiculite in mixed layer minerals. Vermiculite has a much higher CEC (100–150 meq/100 g) than illite (10–40 meq/100 g) and chlorite (10–40 meq/100 g; Grim, 1968), which predominate in the Snowcap samples. However, compared to the values of the pure clay minerals and considering the high clay content of the rocks, CEC values measured on the Leg 193 samples are low and indicate a generally low content of swelling clays.

The higher CEC and surface conductivity of the Roman Ruins samples also affects formation factor. The sample with the largest CEC value (8.9 meq/100 g; sample 1189B-12R-2, 65–67) also has the highest formation factor (143 using Eq. (3)) while the sample with the lowest CEC (0.5 meq/100 g; sample 1188F-25Z-1, 12–14) has the lowest formation factor (76 using Eq. (3)). The difference between the formation factor values derived from Eq. (1), which does not consider surface conductivity, and from Eq. (3), which takes into account surface conductivity, is significantly larger for the Roman Ruins samples than for the samples from the Snowcap field (Table 3).

5.3. Implications for the interpretation of in situ electrical downhole measurements from the PACMANUS hydrothermal field

During ODP Leg 193, downhole logging operations were carried out in several holes (1188B, 1188F, 1189B, and 1189C; Binns et al., 2002). In all holes, electrical resistivity logs show high conductivity values ranging from 0.1 to 11 S/m (Binns et al., 2002). The highest values of electrical conductivity are localized and attributed to interconnected pyrite-rich stockwork mineralization zones (Bartetzko et al., 2003). These zones were mapped by Bartetzko et al. (2003) using a

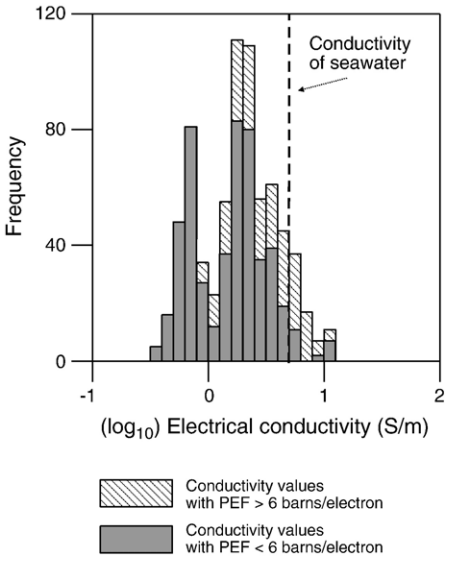

Fig. 6. Sum frequency plot of downhole electrical conductivity data from Hole 1189B. Data are subdivided into two groups using a threshold of 6 barns/e$^-$ in the photoelectric factor log (PEF), a downhole measurement that correlates with the average atomic number of the formation, which was used to map the occurrence of sulfides in the hole by Bartetzko et al. (2003). The histogram shows that high electrical conductivity values are, in many cases, related to photoelectric factor values >6 barns/e$^-$ and thus the presence of sulfide minerals. The occurrence of a few points at high conductivity with low photoelectric factor values may be explained by misclassification due to the very different vertical resolution of the logging tools.

threshold of 6 barns/e$^-$ in the photoelectric factor log as an alternative indicator for the presence of pyrite. Fig. 6 shows that high electrical conductivity values are often related to high photoelectric factor values. Thus, electronic conduction due to the presence of interconnected sulfides, predominantly pyrite, has a controlling effect on the electrical properties of the rocks recovered from Hole 1189B. No samples from the stockwork zone were available for this study and the samples analyzed in this study contain only small amounts of macroscopic pyrite, if any.

Fig. 7 shows a comparison of electrical conductivity measurements from core and from wireline logging data in the deeper part of Hole 1189B. Values measured in the laboratory are lower than values obtained from in situ wireline logging measurements. High-resolution microconductivity images obtained from the Formation MicroScanner™ (FMS) show a clear fracture pattern and the typical texture of vesicular rocks or disseminated sulfides. One explanation for the discrepancy between core and downhole measurements is that logging data integrates over a much larger volume than the core samples. Therefore, downhole measurements tend to measure the higher electrical conductivity values associated with large fractures, sulfide minerals, and alteration clay minerals that may not be present in core samples. Another potential explanation for the disparity between core and log electrical conductivity measurements is the difference in frequency used by the different methods. Electrical conductivity and formation factor values from cores were measured at low frequencies (7.5 to 10 Hz). Induction logging tools such as the Phasor Dual Induction Tool™ (Trademark of Schlumberger) employed during Leg 193 use high frequencies of 20 and 40 kHz. Four of the nine samples analyzed at NER show a significant dependence of electrical conductivity on frequency, i.e. electrical conductivity increases strongly with frequency (Fig. 3). Two of these samples (1188A-9R-1, 118–120 and 1189B-11R-3, 12–14) contain macroscopic pyrite (Iturrino et al., 2004). In particular, sample 1189B-11R-3, 12–14 is representative of a clay-rich interval containing trace amounts of disseminated pyrite (Binns et al., 2002; Iturrino et al., 2004) and this characteristic composition may contribute to the observed frequency dependence. Fig. 7 shows that the conductivity value of the core samples obtained at a higher frequency is

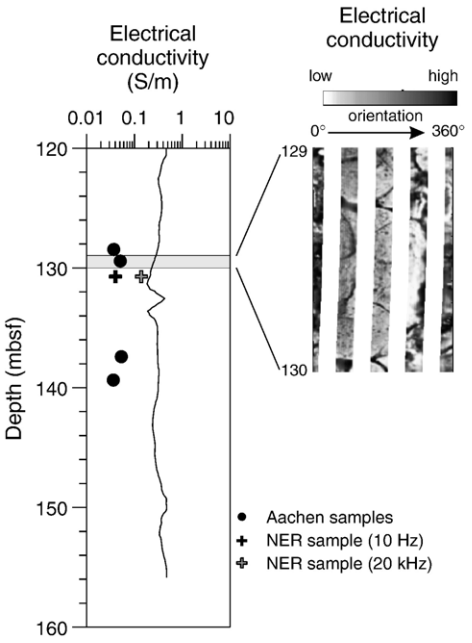

Fig. 7. Comparison of electrical measurements on samples and from in situ downhole measurements in Hole 1189B (Roman Ruins). The left panel shows core data (black dots and crosses) and downhole measurements using a Dual Phasor Induction Tool™ (Trademark of Schlumberger). The right panel shows an example of a microconductivity image carried out with a Formation MicroScanner™ (Trademark of Schlumberger) tool. The high-resolution image show the vesicular and fractured character of the rock. See text for discussion.

closer to the conductivity values from wireline logging data.

Our results show that at PACMANUS, the effects of several conduction mechanisms overlap and make it difficult to compare electrical conductivity data from cores to downhole logging measurements. Therefore, most of the classical interpretation methods for downhole electrical conductivity measurements that are frequently used to compute, for example, porosity profiles using Archie's law in environments where electrical conductivity is mainly controlled by the (connected) pore space, cannot be applied in this environment.

6. Conclusions

We investigated the electrical properties of core samples of hydrothermally altered dacite recovered during ODP Leg 193 at the PACMANUS hydrothermal field. The results of the electrical conductivity measurements presented in this study show that three electric conduction mechanisms are important. Electrolytic conduction through the pore space is mainly controlled by the structure of the rocks. Tortuosity is highly variable because of a large variety in volcanic texture due to a complex volcanic architecture and emplacement history, as well as changes in pore space structure caused by hydrothermal alteration. Surface conduction is controlled by alteration style and the composition of the clay mineral fraction, i.e. the presence of vermiculite in mixed layer clay minerals. The occurrence of disseminated pyrite causes a frequency dependence of electrical conductivity due to polarization processes at the interface between metal and fluid. The overlap of these different conduction mechanisms complicates a comparison of electrical conductivity data between core and logging data and precludes most classical applications of the in situ electrical conductivity logs.

Acknowledgements

This research used data provided by the Ocean Drilling Program (ODP). The ODP is sponsored by the participating countries under management of Joint Oceanographic Institutions (JOI), Inc. Funding by the German Science Foundation to A. Bartetzko and J. Arnold (DFG-Project Ba 2196/1) is gratefully acknowledged. Research by G. Iturrino was funded by USSSP grant #193-F001443. We thank K. Lackschewitz for helpful discussions on clay mineralogy in Leg 193 holes and R. Binns for comments to the manuscript. Comments and suggestions from two anonymous reviewers significantly helped to improve the manuscript.

References

Archie, G.E., 1942. The electrical resistivity log as an aid in determining some reservoir characteristics. Pet. Tech. 5, 1–8.

Bartetzko, A., Paulick, H., Iturrino, G., Arnold, J., 2003. Facies reconstruction of a hydrothermally altered dacite extrusive sequence — evidence from geophysical downhole logging data (ODP Leg 193). Geochem. Geophys. Geosyst. 4, doi:10.1029/2003GC000575.

Binns, R.A., Scott, S.D., 1993. Actively forming polymetallic sulfide deposits associated with felsic rocks in the eastern Manus back-arc basin, Papua New Guinea. Econ. Geol. 88, 2226–2236.

Binns, R.A., Barriga, F.J.A.S., Miller, D.J., et al., 2002. Proceedings of the Ocean Drilling Program, Initial Report 193. Ocean Drilling Program. Texas A&M University, College Station, TX USA, pp. 77845–79547. CD-ROM.

Christiansen, L.B., Iturrino, G.J., 2004. Core-scale permeability of an actively venting, felsic-hosted hydrothermal system: the PACMAUS hydrothermal field. In: Barriga, F.J.A.S., Binns, R.A., Miller, D.J., Herzig, P.M. (Eds.), Proceedings of the Ocean Drilling Program, Scientific Results 193, [Online]. Available from World Wide Web: <http://www-odp.tamu.edu/publications/193_SR/VOLUME/CHAPTERS/202.PDF>.

Grim, R.E., 1968. Clay Mineralogy. International Series in the Earth and Planetary Sciences, 2nd edition. McGraw-Hill.

Guéguen, Y., Palciauskas, V., 1994. Introduction to the Physics of Rocks. Princeton University Press.

Ildefonse, B., Pezard, P., 2001. Electrical properties of slow-spreading ridge gabbros from ODP Site 735, Southwest Indian Ridge. Tectonophysics 330, 69–92.

Iturrino, G.J., Davis, E., Johanson, J., Gröschel-Becker, H., Lewis, T., Chapman, D., Cermak, C., 2000. Permeability, electrical, and thermal properties of sulfide, sedimentary, and basaltic units from the Bent Hill area of Middle Valley, Juan de Fuca Ridge. In: Zierenberg, R.A., Fouquet, Y., Miller, D.J., Normark, W.R. (Eds.), Proceedings of the Ocean Drilling Program, Scientific Results, Ocean Drilling Program, vol. 169. Texas A&M University, College Station, TX USA, pp. 77845–79547. CD-ROM.

Iturrino, G.J., Ketcham, R.A., Christiansen, L., Boitnott, G., 2004. Data report: permeability, resistivity, and X-ray computed tomography measurements in samples from the PACMANUS hydrothermal system. In: Barriga, F.J.A.S., Binns, R.A., Miller, D.J., Herzig, P.M.Proceedings of the Ocean Drilling Program, Scientific Results, vol. 193. [Online]. Available from World Wide Web: <http://www-odp.tamu.edu/publications/193_SR/205/205.htm>.

Jackson, P.D., Taylor Smiths, D., Standford, P.N., 1978. Resistivity–porosity–particle shape relationships for marine sands. Geophysics 43, 1250–1268.

Jarrard, R.D., Schaar, R., 1991. Electrical properties of basalts from Sites 768 and 770. In: Silver, E.A., Rangin, C., von Breymann, M.T., et al.,Proceedings of the Ocean Drilling Program, Scientific Results, vol. 124. Ocean Drilling Program, College Station, TX, pp. 91–104.

Kan, R., Sen, P.N., 1987. Electrolytic conduction in periodic arrays of insulators with charges. J. Chem. Phys. 86, 5748–5756.

Kaufhold, S., Penner, D., 2004. Bewertung der Anwendbarkeit der SER-Methode zur Qualitätskontrolle von Westerwälder Tonen.

Presented at the Annual Meeting of the German–Austrian–Swiss Clay Group Association, 20–21 September 2004, Karlsruhe.

Ketcham, R.A., Iturrino, G.J., 2005. Nondestructive high-resolution visualization and measurement of anisotropic effective porosity in complex lithologies using high-resolution X-ray computed tomography. J. Hydrol. 302, 92–106.

Lackschewitz, K.S., Devey, C.W., Stoffers, P., Botz, R., Eisenhauer, A., Kummetz, M., Schmidt, M., Singer, A., 2004. Mineralogical, geochemical and isotopic characteristics of hydrothermal alteration processes in the active PACMANUS hydrothermal field hosted by felsic volcanic rocks, Manus Basin, Papua New Guinea. Geochim. Cosmochim. Acta 68, 4405–4427.

Lockner, D.A., Byerlee, J.D., 1985. Complex resistivity measurements of confined rock. J. Geophys. Res. 90, 7837–7847.

Meier, L.P., Kahr, G., 1999. Determination of the cation exchange capacity of clay minerals based on the complexes of the copper (II)ion with triethylenetetramine and tetraethylenepentamine. Clays Clay Miner. 47, 386–388.

Mendelson, K.S., Cohen, M.H., 1982. The effect of grain anisotropy on the electrical properties of sedimentary rocks. Geophysics 7, 257–263.

Micromeritics, 2001a. AccuPyc™ 1330 Manual—V3.03. Micromeritics.

Micromeritics, 2001b. GeoPyc™ 1360 Manual—V3.01. Micromeritics.

Patchett, J.G., 1975. An Investigation of Shale Conductivity. Transactions of SPWLA 16th Annual Logging Symposium Houston Texas. June 4–7, Paper V.

Paulick, H., Vanko, D.A., Yeats, C.J., 2004. Drill core-based facies reconstruction of a deep-marine, felsic volcano hosting an active hydrothermal system (Pual Ridge, Papua New Guinea, ODP Leg 193). J. Volcanol. Geotherm. Res. 30, 31–50.

Pelton,W.H., 1977. Interpretation of complex resistivity and dielectric data. Ph.D. thesis, Univ. Utah.

Pezard, P.A., 1990. Electrical properties of Mid-Ocean Ridge Basalt and implications for the structure of the upper oceanic crust in Hole 504B. J. Geophys. Res. 95, 9237–9264.

Purvance, D.T., Andricevic, R., 2000. On the electrical–hydraulic conductivity correlation in aquifers. Water Resour. Res. 36, 2905–2913.

Rangin, C., Silver, E.A., von Breymann, M.T., et al., 1990. Proceedings of the Ocean Drilling Program, Initial Reports, vol. 124. Ocean Drilling Program, College Station, TX.

Ransom, R.C., 1984. A contribution toward a better understanding of the modified Archie formation resistivity factor relationship. Log Anal. 25, 7–12.

Revil, A., Cathles III, L.M., Losh, S., Nunn, J.A., 1998. Electrical conductivity in shaly sands with geophysical applications. J. Geophys. Res. 103, 23925–23936.

Revil, A., Hermitte, D., Spangenberg, E., Cochemé, J.J., 2002. Electrical properties of zeolitized volcanic materials. J. Geophys. Res. 107 (B8), doi:10.1029/2001JB000599.

Saar, M.O., Manga, M., 1999. Permeability–porosity relationship in vesicular basalts. Geophys. Res. Lett. 26, 111–114.

Smith, J.V., Miyake, Y., Oikawa, T., 2001. Interpretation of porosity in dacite lava domes as ductile–brittle failure textures. J. Volcanol. Geotherm. Res. 112, 25–35.

Sruoga, P., Rubinstein, N., Hinterwimmer, G., 2004. Porosity and permeability in volcanic rocks: a case study on the Serie Tobifera, South Patagonia, Argentina. J. Volcanol. Geotherm. Res. 132, 31–43.

Titov, K., Komarov, V., Tarasov, A., Levitski, A., 2002. Theoretical and experimental study of time domain induced polarization (IP) in water-saturated sands. J. Appl. Geophys. 50, 417–433.

Van Brakel, J., Heertjes, P.M., 1974. Analysis and diffusion in macroporous media in terms of a porosity, a tortuosity and a constrictivity factor. Int. J. Heat Mass Transfer 17, 1093–1103.